Copper $L_{2,3}$ near-edge structure in Cu_2O

S. L. Hulbert, B. A. Bunker, and F. C. Brown
Department of Physics and Materials Research Laboratory, University of Illinois at Urbana-Champaign, 1110 W. Green St., Urbana, Illinois

P. Pianetta
Stanford Synchrotron Radiation Laboratory, Stanford, California 94305
(Received 24 February 1984)

We report on high-resolution total-yield measurements of the Cu $L_{2,3}$ absorption edge in Cu_2O using the JUMBO monochromator at the Stanford Synchrotron Radiation Laboratory. Care was taken to prepare the surface of a well-characterized single crystal, rather than use oxidized copper. A comparison was also made with electron-energy-loss spectra (transmission of a thin Cu_2O crystal). Prominent white lines or core excitons appear at the spin-orbit-split Cu L_3 (931 eV) and L_2 (951 eV) thresholds. These edge features are like those observed in CuO (even though the Cu d states are filled in Cu_2O) but are asymmetrically broadened on the high-energy side, probably due to more than one component. The core binding energy is measured by photoemission, and local states are compared with transitions to the continuum. We believe that the strong edge features in Cu_2O can be understood in part as transitions to antibonding molecular-orbital states of the linear O-Cu-O molecular cluster peculiar to copper in the Cu_2O crystal structure.

I. INTRODUCTION

Cuprous oxide is a canonical exciton material. The oxygen $2p$ and copper $3d$ shells are filled in Cu_2O, and a direct band gap of 2.22 eV occurs between a d-like valence band and a conduction-band minimum of largely s character on the copper.[1,2] Optical absorption shows two series of forbidden excitons, followed by two series of allowed excitons with Rydberg constants in the range 50—150 meV. These series have been thoroughly studied using one-[3] and two-photon spectroscopy,[4] as well as the resonant Raman effect.[5] These are Wannier excitons, and the early effective-mass theory of Elliot[6] has been notably successful.

The question naturally arises: Do excitons influence near-edge structure for transitions of inner-shell electrons? Calculated and experimental core-level binding energies are given for Cu_2O in Table I. Cuprous oxide is ideal for studying *core excitons* at the Cu $2p$ ($L_{2,3}$) and $3p$ ($M_{2,3}$) core thresholds since transitions to s-like final states (conduction-band minimum) are dipole allowed.

The transition-metal oxides with unoccupied d states, e.g., TiO_2, Cr_2O_3, FeO, NiO, and CuO, show prominent resonances or "white lines" at the metal L thresholds.[7] On the other hand, copper metal does not show a singularity at the L edge presumably because of filled d shells. Cuprous oxide Cu_2O also has little unoccupied d-state density; consequently the usual criterion for appearance of

TABLE I. Dispersionless core energy levels of Cu^+ and O (O^{2-} is not stable by itself) calculated using a relativistic Herman-Skillman routine and their Madelung-corrected (+12.78 eV for Cu^+ and −21.89 eV for O) values. XPS binding energies for Cu_2O obtained using 1200 eV photons from SPEAR. Ranges of calculated band energies at Γ (Ref. 2). All energies are referred to the valence-band maximum.

Core level	Atomic level energy (eV)	Madelung corrected energy (eV)	XPS binding energy (eV)	Calculated band energies at Γ (eV)
Cu $1s$	−8953.6	−8940.8		
Cu $2s$	−1096.0	−1083.3	1071.5	
Cu $2p_{1/2}$	−968.5	−955.7	951.6	
Cu $2p_{3/2}$	−947.3	−934.5	931.7	
O $1s$	−537.3	−559.2	529.0	
Cu $3s$	−131.2	−118.4	119.5	
Cu $3p_{1/2}$	−90.4	−77.6	75.3	
Cu $3p_{3/2}$	−87.7	−74.9	75.3	
O $2s$				−22.0
O $2p$				−7.6 to −4.4
Cu $3d$				−2.4 to 0.0

a white line, namely d-like conduction bands,[8] is absent. On the other hand, Cu_2O has a very open crystal structure with a strong redistribution of charge which might tend to favor local atomiclike excitations. The crystal structure of Cu_2O is simple cubic, space group O_h^4 (cuprite) with two oxygen atoms and four Cu atoms per unit cell. The cubic lattice parameter is $a=4.27$ Å. As shown in Fig. 1, each oxygen atom is surrounded by a tetrahedron of Cu atoms and each Cu atom is twofold coordinated by oxygen atoms in an open O-Cu-O linear geometry.

Bassani has approached the problem of explaining core excitons in semiconductors by using an effective-mass Hamiltonian which includes dynamical screening and polarization effects.[9] Minimization of this Hamiltonian for core excitons can lead to a much stronger electron-hole interaction than that associated with static screening. In a sense the effective-mass approximation (EMA) breaks down, leading to core-exciton binding energies of the order of 1 eV as compared to valence-exciton binding energies in the same material of the order of 0.1 eV or less. Within the framework of polaron theory this breakdown, the so-called shallow-deep instability, corresponds to the electronic polaron radius becoming larger than the exciton radius.

According to Bassani,[9] the basic requirements for breakdown of the EMA are (1) a large conduction-band electron effective mass m/m_e and (2) a small electron dielectric function ϵ_e (other more subtle effects such as valley-valley interaction can produce such a breakdown in materials with small m/m_e or large ϵ_e). The relevant parameters for a number of materials are given in Table II. Also shown is a parameter η, as defined in Table II, which indicates whether the electron-core hole interaction is fully screened ($\eta>1$ shallow exciton) or partially screened ($\eta<1$ deep excitons). Notice that Cu_2O has $\eta=1.3$ and is therefore on the borderline between full static screening and dynamically reduced screening. Cuprous oxide is a prime candidate for reduced screening because its electron dielectric function ($\epsilon=6.23$) is a factor of 2 smaller than that of the classic semiconductors Ge and GaAs and its conduction-band effective mass ($0.61m_e$) is 1 order of magnitude greater than that of GaAs and 5 times larger than that of Ge. The s-like (Γ_6^+) conduction-band minimum in Cu_2O (to which transitions from the Cu $2p$ core level are dipole allowed) makes it a good candidate for exhibiting reduced screening of the

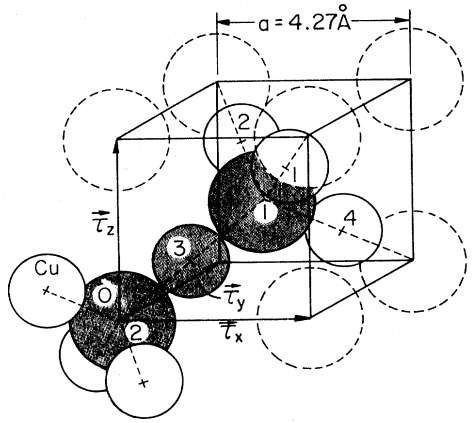

FIG. 1. Cubic unit cell of the cuprite crystal structure (space group O_h^4), to which Cu_2O belongs, showing its basic translation vectors $\vec{\tau}_x=a(1,0,0)$, $\vec{\tau}_y=a(0,1,0)$, and $\vec{\tau}_z=a(0,0,1)$.

$n=1$ line. The $n=2,3,\ldots$ exciton series should be more fully screened. Ideally, the separate members of the exciton series would be observed merging into the continuum absorption at threshold. However lifetime broadening of the Cu $2p$ core level is expected to erase the fine structure of this excitonic series, excitonic enhancement at threshold should occur as discussed by Altarelli and Dexter.[10]

Recently, Robertson[2] has evaluated the possibility of a deep or local exciton state near the copper $L_{2,3}$ edge in Cu_2O. For this purpose a Koster-Slater tight-binding impurity calculation was carried out as first used for excitons by Hjalmarson, Büttner, and Dow.[11] A local state is found in Cu_2O, although it appears to be a resonance very close to threshold. Robertson points out that his prediction of the *existence* of such a state is stronger than its absolute energy relative to threshold.

On the experimental side, some low-resolution energy-loss data exist for the Cu $M_{2,3}$ threshold at 75 eV,[12] and total-yield data on the oxygen K edge has been recently reported.[13] Except for the early data of Bonnelle,[14] the copper $L_{2,3}$ thresholds of Cu_2O, which lie in the intractable region around 930 eV, have been seldom studied. The present work presents a high-resolution total-yield measurement (proportional to absorption coefficient) on a

TABLE II. The parameters a (unit-cell dimension), ϵ_e (electronic dielectric constant), ϵ_0 (static dielectric constant), m_1/m (m_1 is the conduction-band effective mass, m is the bare electron mass), k_M (radius of a sphere with volume equal to that of the Brillouin zone), and $\eta=(m/m_1)(a_0/\pi)k_M(\epsilon_e/\epsilon^*)$, where $1/\epsilon^*=1/\epsilon_\infty+1/\epsilon_e$, for various representative semiconductors and insulators from Ref. 9. $\eta>1$ indicates fully screened (static) electron-hole interaction and $\eta<1$ indicates reduced screening (dynamic) in the central cell. The nature of screening for materials with $\eta\simeq1$ is not determined by this model.

Crystal	Structure	a (Å)	ϵ_e	ϵ_0	ϵ^*	m_1/m	k_M (Å^{-1})	η
Ge	diamond	5.65	15.36	15.36	1.070	0.12	1.10	22.2
GaAs	zincblende	5.65	10.90	12.90	1.101	0.066	1.10	27.8
Si	diamond	5.43	11.4	11.4	1.096	0.258	1.14	7.8
CdTe	zincblende	6.48	7.20	10.9	1.161	0.11	0.95	9.0
CuCl	zincblende	5.42	3.70	7.4	1.370	0.44	1.14	1.2
Cu_2O	cubic	4.27	6.23	7.1	1.191	0.61	0.91	1.3
Ar	fcc	5.31	1.66	1.66	2.515	0.5	1.16	0.26

single crystal of Cu_2O in the energy range of Cu $L_{2,3}$ edges. Partial electron yield and the various secondary electron channels are also explored. In addition a certain amount of electron-energy-loss data was taken in transmission on a thin section of the Cu_2O crystal. Experimental details and results are given in the next section. Contrary to expectation, strong white lines do appear at the copper $L_{2,3}$ edge in Cu_2O and they are interpreted as relatively local core excitons.

II. EXPERIMENTAL RESULTS

The samples used were (100) slices cut from a single-crystal boule of Cu_2O prepared by a zone-refining technique at 1600 °C in a 0.6-Torr oxygen atmosphere.[15] They appeared clear and deep red in color due to the 2.2-eV band gap. The sample surface was polished using a series of grits ending with 0.1-μm alumina. Following a light etch the samples were mounted in ultrahigh vacuum. *In situ* sputtering with 30 mA of 0.5-kV argon ions for 10 min was sufficient to remove surface contamination. Heating and repeated sputtering did not increase the strength of the x-ray photoelectron spectral (XPS) features relative to background and also did not change the positions or shapes of the partial- and total-yield features.

The total yield from a pure crystalline sample of Cu_2O in the energy range of the Cu $L_{2,3}$ edge is shown in Fig. 2. Notice the strong resonance or core-exciton line at 931.0 eV. This feature is separated from the L_2 edge (950.9 eV) by the XPS-determined $L_{2,3}$ spin-orbit splitting of 19.9 eV. The L_3:L_2 amplitude ratio is close to the statistical value of 2:1. Although we are dealing with photoelectron emission, total yield is believed to be a reliable measure of the bulk absorption coefficient of a solid.[16]

The yield spectrum shown in Fig. 2 was taken using the double-crystal monochromator JUMBO (Ref. 17) at the Stanford Synchrotron Radiation Laboratory during dedicated operation of SPEAR at 3 GeV with a stored electron current of 74 mA. A JUMBO user can select from any of four sets of diffracting crystals, e.g., beryl ($10\bar{1}0$), α-quartz ($10\bar{1}0$), InSb(111), and Si(111), which provide overlapping energy scan ranges from 500—4000 eV. With the use of a pair of large d-spacing beryl crystals ($2d = 15.96$ Å), JUMBO provides an energy resolution of $\simeq$0.6 eV [full width at half maximum (FWHM)] at the Cu $L_{2,3}$ edge ($\simeq$930 eV). Figure 2 was obtained under these conditions.

Both total electron yield (using a +2400-V biased channeltron near the sample) and Cu $L_3M_{4,5}M_{4,5}$ Auger partial-electron-yield data (using a PHI double-pass cylindrical mirror analyzer (CMA)] were collected simultaneously and digitally divided by total-yield data from a gold monitor located just before the sample chamber. The total- and Auger partial-yield spectra agree with respect to the L_2 and L_3 edge shapes and step heights but the Auger yield increases more steeply above the L_3 edge than does the total yield due to increasing strength in the $L_3M_{4,5}M_{4,5}$ channel. All data were digitally recorded and processed on a VAX computer using interactive graphics programs.

Careful characterization of our sample by XPS confirmed that the chemical composition of its surface was indeed Cu_2O and not CuO. For example, Fig. 3 shows an electron distribution curve (EDC) for Cu_2O over a wide energy range using 1200-eV photons from SPEAR as an excitation source. Similar data taken with Mg $K\alpha$ radiation (1253.6 eV) are shown on an expanded scale for Cu_2O in Fig. 4(a) and for CuO in Fig. 4(b).[18] The measured Cu L_3 binding energy in Cu_2O (931.7 eV) is less than that in metal (932.4 eV), whereas the published L_3 binding energy for CuO ($\simeq$933.6 eV) is larger than in the pure metal. In addition, the measured full width at half maximum of the Cu L_3 peak in Cu_2O ($\simeq$2 eV) agrees with that measured by Schon[19] (1.8 eV), which is a factor of 2 less than the value he measured for CuO (3.7 eV). Furthermore, the measured Cu $L_{2,3}$ XPS spectrum of Cu_2O [Fig. 4(a)] does not contain the prominent shake-up (multielectron excitation) satellite peaks at 943 and 963 eV which are characteristic of CuO.[20] Refer to Fig. 4(b).

The measured valence spectrum of our samples (not shown) has peaks at $\simeq$3 eV (Cu $3d$) and $\simeq$6 eV (O $2p$) below the valence-band maximum in agreement with the

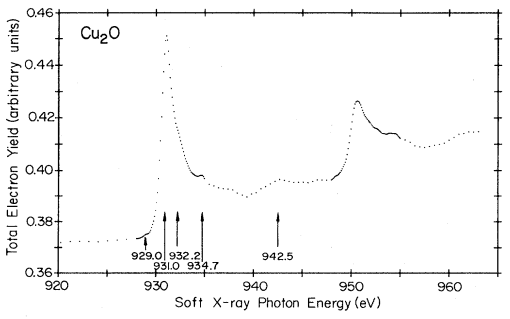

FIG. 2. Total-yield spectrum from a pure crystalline sample of Cu_2O in the energy range of the Cu $L_{2,3}$ absorption edge. Total yield is a reliable measure of the bulk absorption coefficient of a solid (Ref. 16).

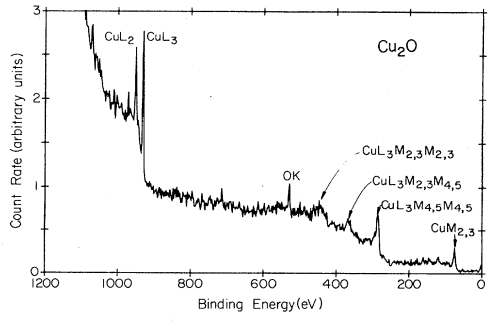

FIG. 3. Wide-range electron distribution curve (EDC) for Cu_2O using 1200-eV photons from SPEAR as the excitation source. The Cu $L_{2,3}$, O K, Cu M_1, and Cu $M_{2,3}$ core levels and the Cu $L_3M_{4,5}M_{4,5}$, Cu $L_3M_{2,3}M_{4,5}$, and Cu $L_3M_{2,3}M_{2,3}$ Auger lines.

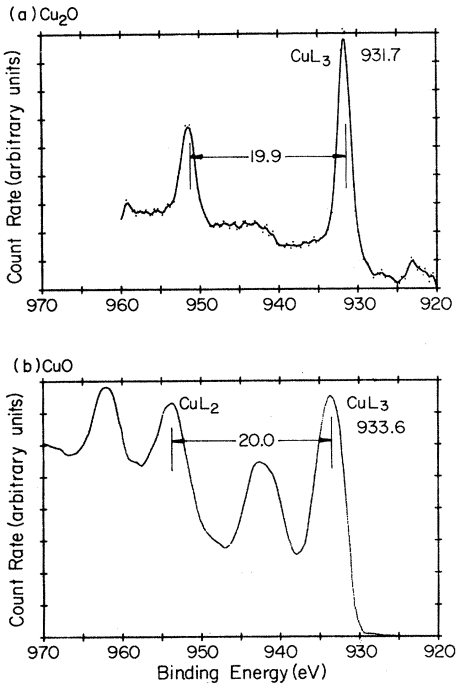

FIG. 4. Cu $L_{2,3}$ EDC's for (a) Cu_2O and (b) CuO (Ref. 18) using Mg $K\alpha$ radiation (1253.6 eV) as the excitation source.

ultraviolet photoelectron valence spectra for Cu_2O by Benndorf *et al.*[12] Finally, the measured kinetic energy of the Cu $L_3M_{4,5}M_{4,5}$ Auger line (917.3 eV) in Cu_2O agrees with the published values and is less than that of CuO (917.9 eV).[19] Table III consolidates these published and measured XPS energies for Cu, CuO, and Cu_2O.

As an additional check we measured the electron-energy-loss spectrum (EELS) on an ion-milled ($\simeq$400 Å thick) section of the same sample of Cu_2O that was used for the total-yield measurements. For this purpose a Philips EM420 electron microscope was employed. The EELS spectrum of Cu_2O reproduces, with less resolution, the exact positions and general shapes of the features in the total-yield spectrum of Fig. 2. In fact, the total-yield data of Fig. 2 broadened and smoothed by a 2-eV triangular window is nearly identical in shape to the transmission EELS spectrum. The bulk nature of the transmission EELS technique gives us confidence that the yield of 1-keV electrons shown in Fig. 2 is a bulk probe of the electronic structure of Cu_2O. We turn to a discussion of the near-edge data of Fig. 2 in the next section.

III. DISCUSSION AND CONCLUSION

Close inspection of Fig. 2 shows that the various spectral features can be separated into two groups corresponding to an $L_{2,3}$ spin-orbit splitting of 19.9±0.1 eV. These various features are listed in Table IV. The main band or core-exciton line occurs at 931.0 eV with a spin-orbit partner at 950.9 eV. We suggest it is fortuitous that this white line appears at nearly the same energy as in the energy-loss data on CuO.[7] Actually, the near-edge data in Cu_2O and CuO are qualitatively different. Although of similar strength compared to Cu_2O, the white line in CuO is symmetric whereas the edge feature in Cu_2O is narrower and asymmetrically broadened on the high-energy side. Furthermore, the CuO spectrum contains a small broad band at 939 eV, while that of Cu_2O contains a small sharp peak at 934.7 eV and a small broad feature at 942.5 eV.

Leapman *et al.*[7] note that the ratio of the white-line peak height to L_3 absorption step in CuO (d^9 configuration) is the smallest of the third-row transition-metal-oxide series (TiO_2, Cr_2O_3, FeO, NiO, and CuO) due to the nearly filled Cu $3d$ shell in CuO. In molecular-orbital terms the Cu $3d$-derived $2t_{2g}$ and $3e_g$ antibonding molecular orbitals are both empty in TiO_2 as compared to one electron from full in CuO. On the basis of this inverse relation between white-line strength and Cu $3d$ shell filling, the filled Cu $3d^{10}$ configuration in Cu_2O should preclude the existence of a white line such as that observed in the L_3 near-edge absorption structure of CuO. Actually the white line observed at threshold in Cu_2O is about as strong as in CuO.

As far as the main 931.0-eV line and its spin-orbit partner are concerned, it would appear that a local molecular approach is an appropriate starting point. In fact, the copper atom and its two oxygen neighbors closely resemble a linear SO_2 molecule whose $L_{2,3}$ threshold spectrum is known to be quite singular.[21] The scattering of outgoing partial waves ($s,p,d,\ldots$ character) associated with an electron ejected by photoexcitation from the central atom can be used to predict the near-edge absorption of the cluster. This multiple-scattering approach has

TABLE III. Cu L_3 binding energies and Cu $L_3M_{4,5}M_{4,5}$ Auger kinetic energies for Cu and its oxides CuO and Cu_2O. The uncertainty of the published values represent the spread in the values reported in the literature as compiled by Muilenberg *et al.* (Ref. 18) and others. The last column gives measured kinetic energies of these and other Cu and O Auger transitions in Cu_2O. All energies in eV.

	Cu (published)	CuO (published)	Cu_2O (published)	Cu_2O (measured)
E^b(Cu L_3)	932.4±0.2	933.3±0.3	932.2±0.0	931.7
E_{kin}^{Aug}(Cu $L_3M_{4,5}M_{4,5}$)	918.8±0.3	918.0±0.2	917.3±0.4	917.3
E_{kin}^{Aug}(Cu $L_3M_{2,3}M_{4,5}$)				832.0
E_{kin}^{Aug}(Cu $L_3M_{2,3}M_{2,3}$)				754.0
E_{kin}^{Aug}(O KVV)				485.0

TABLE IV. Spectral features observed in the $L_{2,3}$ near-edge absorption spectrum (total yield) for crystalline Cu_2O. Energy uncertainties ±0.1 eV.

Energy (eV)	Core level	Tentative identification
929.0	L_3	weak precursor, triplet state?
931.0	L_3	$n=1$ core exciton, $3a_{1g}$
932.0	L_3	secondary band, $2a_{2u}$
934.7	L_3	$n=2$ and higher final states unresolved continuum threshold
942.5	L_3	Cu s-p DOS peak
948.9	L_2	weak precursor?
950.9	L_2	$n=1$ core exciton, $3a_{1g}$
952.1	L_2	secondary band, $2a_{2u}$
954.6	L_2	$n=2$ plus unresolved continuum
962.4	L_2	Cu s-p DOS peak

proved successful in describing core-level absorption in a variety of simple and complex molecular systems, e.g., N_2, CO, and NO by Dehmer[22] and $GeCl_4$ and GeH_4 by Doniach and co-workers.[23] Recently, a more sophisticated version of this approach has been used by Durham *et. al*[24] and Pendry[25] to predict x-ray absorption near-edge structure (XANES) in various solids, including some without long-range order, e.g., glasses and other amorphous materials. Currently the feeling is that more structural information, e.g., locations and site symmetries of the atoms in a particular shell, is contained in the XANES region of an edge absorption spectrum than in the extended x-ray absorption fine structure (EXAFS). However, the large cluster size ($\simeq 10^2$ atoms) required for XANES calculations makes them very time consuming. It would be worthwhile to compare both single- and multipole-scattering XANES calculations for Cu_2O with our measured spectrum, although multielectron features such as effective-mass-like excitons are not included in the multiple-scattering calculation.

As a zeroth-order molecular (as opposed to solid-state) approach to the near-edge absorption features in Cu_2O, one can guess the ordering of the molecular orbitals in the $(CuO_2)^{3-}$ molecule, which consists of a Cu^+ ion and its two O^{2-} nearest neighbors. Considering only the symmetry operations of the full Cu_2O lattice at the Cu site (point group D_{3d}) one obtains the reducible representations for the valence orbitals of Cu ($3d$, $4s$, and $4p$) and O ($2p$) in the linear O-Cu-O geometry. Mixing the atomic orbitals of each symmetry using a linear combination of atomic-orbitals approach produces the tentative molecular-orbital diagram for $(CuO_2)^{3-}$ shown in Fig. 5. The 10 Cu^+ and 12 O^{2-} valence electrons fill the bonding, $2e_g$ nonbonding, and $3e_g$ hybrid antibonding molecular orbitals, leaving the antibonding $3a_{1g}$, $2a_{2u}$, and $2e_u$ molecular orbitals unfilled. In solid-state terms, the conduction-band partial density of states (PDOS) should be mainly Cu s- and Cu p-like near threshold with a peak in the Cu p-like PDOS at higher energy. The Cu d PDOS is finite but should be relatively small near the bottom of the conduction band. This statement is in qualitative agreement with the partial density-of-states calculation of Robertson.[2]

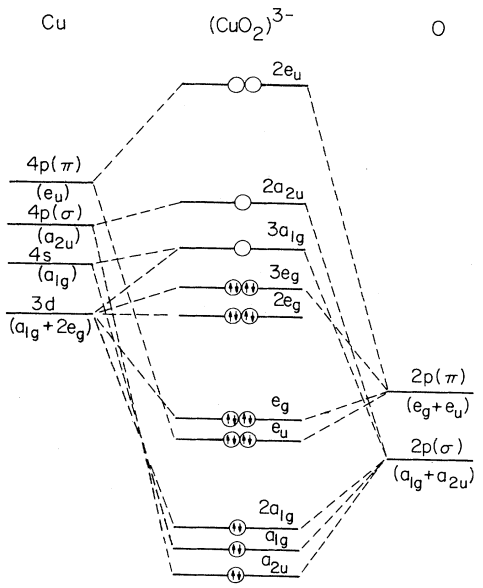

FIG. 5. Molecular-orbital diagram for Cu_2O showing Cu and O atomic orbitals and the resultant molecular orbitals and their occupations in the ground state. The symmetry of the full lattice at the Cu site in Cu_2O is D_{3d}.

Since p-like initial states (e.g., Cu $L_{2,3}$) select d- and s-like final states in the dipole approximation, the Cu $L_{2,3}$ near-edge absorption structure is expected to exhibit a peak corresponding to the s-like unfilled molecular orbital in Fig. 5, namely the $3a_{1g}$ antibonding molecular orbital. The very compact nature of the initial-state wave function (Cu $2p$) can lead to a strong, sharp excitonic transition to a $3a_{1g}$ molecular-orbital final state if the final state is also compact (i.e., if there is strong wave-function overlap in the region of the localized $2p$ core hole).

This tentative molecular-orbital scheme can be compared with published Cu K and O K near-edge absorption spectra for Cu_2O. For example, x-ray photographic plate microphotometer traces for the Cu K edge in Cu_2O show little or no evidence of a peak (or white line) at threshold.[26–28] This is consistent with the fact that transitions to the localized $3a_{1g}$ unoccupied molecular orbital in Fig. 5 are dipole forbidden from the Cu $1s$ core level. Dipole-allowed transitions to the unoccupied $2a_{2u}$ molecular orbital could account for the observation of a weak white line at threshold in Ref. 26. Transitions to all three unoccupied molecular orbitals in Fig. 5 are dipole allowed from the O K level in Cu_2O. Several features occur in the recently observed spectrum,[13] a sharp peak at threshold (O $1s \rightarrow 3a_{1g}$) followed by a broad peak at $\simeq 8$ eV higher energy (O $1s \rightarrow 2e_u$) and one or two additional bands at still higher energy. To summarize the copper L-edge data, we assign the main peak at 931.0 eV to a Frenkel-like core exciton. In molecular terminology this is a transition from the Cu $2p$ to the a_{1g} molecular orbital. The asymmetric shape of this line and the higher-energy structure will now be discussed.

The sharpness of the small peak at 934.7 eV in Fig. 2 indicates that the associated transition might be due to a

bound final state. It is reasonable to suggest that this peak is the barely resolved $n=2$ member of an exciton series bound to the s-like conduction-band minimum in Cu_2O. Figure 6 shows the measured total-yield curve and a Lorentzian-broadened (FWHM $\Gamma=0.6$ eV) exciton series fit [curve (a)] according to a modified Elliot theory.[6] For this purpose we chose a continuum threshold $E_g=935.2$ eV, an effective Rydberg $R_{\rm eff}=2$ eV for the $n=2,3,\ldots$ members and a central cell (CC) effective Rydberg $R_{\rm eff}^{\rm CC}=4.2$ eV for the $n=1$ member of the series. The absorption profile produced by such a fit is given by[10]

$$\mu(\hbar\omega)=2R\frac{\Gamma/2\pi}{[\hbar\omega-(E_g-R_{\rm eff}^{\rm CC})]^2+(\Gamma/2)^2}+2R\sum_{n=2}^{\infty}\frac{1}{n^3}\frac{\Gamma/2\pi}{[\hbar\omega-(E_g-R_{\rm eff}/n^2)]^2+(\Gamma/2)^2}+\int_{E_g}^{\infty}\frac{1}{1-e^{-\pi\gamma}}\frac{\Gamma/2\pi}{(\hbar\Omega-\hbar\omega)^2+(\Gamma/2)^2}d(\hbar\Omega)\,, \quad (1)$$

where $\gamma=[R/(\hbar\Omega-E_g)]^{1/2}$. In this analysis the continuum is strongly enhanced for many rydbergs above the chosen E_g threshold and a fit is made to the step height in the continuum. A simple $(E-E_g)^{1/2}$ parabolic band absorption is shown for comparison [curve (c)].

In making the fit of Fig. 6 we assume that the asymmetry of the main band is due to the superposition of two peaks, one at 931.0 eV and the other a barely resolved broad band at 932.2 eV [curve (b)]. Assuming that this higher band does not belong to the principal series, it is subtracted off. One possibility is that the 931.0-eV line and higher series is associated with the $3a_{1g}$ final state (mainly s character refer to Fig. 5) and the 932.2-eV band with the $2a_{2u}$ molecular orbital, of mixed s-p character. The broad feature at 942.5 eV is attributed to the $2e_u$ molecular orbital or to higher-band density of states. Another possibility is that we are dealing with a Fano profile due to autoionization or configuration interaction. The shape, however, is not really right for such an assignment, in fact the 932.2-eV peak is almost resolved on the high-energy side of the main band. We prefer to associate it with the local $(2a_{2u})$ final state. These tentative assignments are summarized in Table IV.

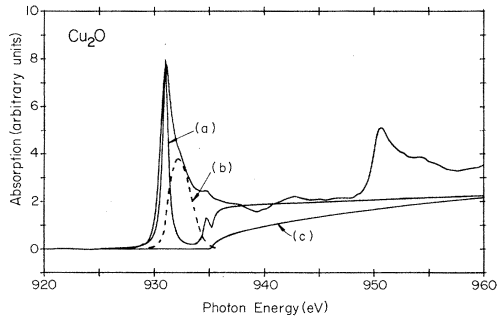

FIG. 6. Wannier exciton series fit, using a modified Elliot[6,10] theory, to the measured Cu $L_{2,3}$ total-yield date of Fig. 1. Fit parameters are continuum threshold $E_g=935.2$ eV, effective Rydberg for $n=2,3,\ldots$ members $R_{\rm eff}=2$ eV, central-cell effective Rydberg for the $n=1$ member $R_{\rm eff}^{\rm CC}=4.2$ eV, and FWHM Lorentzian broadening $\Gamma=0.6$ eV. Simple parabolic band absorption profile proportional to $(E-E_g)^{1/2}$ for comparison with exciton-enhanced threshold profile.

The constants chosen for the fit of Fig. 6 appear somewhat arbitrary. Clearly the central-cell Rydberg $R_{\rm eff}^{\rm CC}=4.2$ eV is large. On the other hand, several volts is reasonable for a highly local molecular-orbital excitation. The higher members of the series also have a rather large effective Rydberg $R_{\rm eff}\sim 2$ eV, but the overall fit to main features of the spectrum is quite good. Even the chosen continuum threshold is in reasonable agreement with the so-called additivity principle.[29] For this purpose the core-exciton binding energy E_c^b is taken as

$$E_c^b=(\delta+E_{cv}+E_g)-E(\hbar\omega)\,, \quad (2)$$

where E_{cv} is the core to maximum valence-band energy (measured by photoemission), E_g is the band gap, and $E(\hbar\omega)$ is the exciton photoabsorption energy. Here the constant δ is a small correction associated with altered screening of the core hole when an electron is in an excitonic final state. Zunger[30] has argued that $\delta\neq 0$ for semiconductors such as GaP and GaAs. The correction δ does appear to be relatively small for alkali halides such as RbCl (Ref. 31) and LiF (Ref. 32). In the present case, $E_{cv}+E_g=931.7+2.2=933.9$ eV, where E_{cv} is directly measured (refer to Fig. 3 and Table III). Comparing with the value $E_g=935.2$ required in the fit of Fig. 6, we suggest that in Cu_2O $\delta\sim 1.3$ eV for the L_3 exciton transition.

In summary, a strong white line has been observed at the Cu $L_{2,3}$ edge in Cu_2O. We refer to this feature at 931.0 eV as a rather local exciton. It can be fairly stated that Cu_2O exhibits a shallow-deep instability at this edge since this peak at threshold (931.0 eV) appears to be well below any reasonably chosen continuum threshold. A purely effective-mass approach using the modified Elliot theory is not satisfactory for the first, nor even for higher, near-edge features. In fact a molecular-orbital or local cluster approach may be a better starting point for a detailed understanding of the $L_{2,3}$ near-edge structure in Cu_2O. This same edge in copper metal does not show a white line,[7] presumably because of screening and the fact that the d shell is filled. Cuprous oxide has a relatively open structure and the way in which charge is redistributed is crucial. The observations on Cu_2O show a number of partially resolved components, and further work on samples at low temperature would be most interesting. Finally, preliminary results of a detailed cluster calculation by Keegstra and Kunz[33] are encouraging. In this approach the ground and excited states of a Cu atom embedded in a charge-neutral lattice that simulates the Cu site symmetry and charge distribution of Cu_2O are computed.

ACKNOWLEDGMENTS

The authors would like to acknowledge the support of the National Science Foundation under Grant Nos. NSF DMR 82-13068 and NSF DMR 80-20250. The Stanford Synchrotron Radiation Laboratory is supported in part by the U. S. Department of Energy. Crystal preparation by Professor A. Compaan is much appreciated, and we would also like to thank M. Mochel and K. Stolt for several measurements and sample characterizations.

[1]L. Kleinman and K. Mednick, Phys. Rev. B **21**, 1549 (1980).
[2]J. Robertson, Phys. Rev. B **28**, 3378 (1983).
[3]S. Nikitine, *Progress in Semiconductors,* edited by A. F. Gibson, R. E. Burgess, and F. A. Kröger (Heywood, London, 1962), Vol. VI, p. 233.
[4]D. Frohlich, R. Kenklies, Ch. Uihlein, and C. Schwab, Phys. Rev. Lett. **43**, 1260 (1979).
[5]M. A. Washington, A. Z. Genack, H. Z. Cummins, R. H. Bruce, A. Compaan, and R. A. Forman, Phys. Rev. B **15**, 2145 (1977).
[6]R. J. Elliot, Phys. Rev. **108**, 1384 (1957).
[7]R. D. Leapman, L. A. Grunes, and P. L. Fejes, Phys. Rev. B **26**, 614 (1982).
[8]M. Brown, R. E. Peierls, and E. A. Stern, Phys. Rev. B **15**, 738 (1977).
[9]F. Bassani, Appl. Opt. **19**, 4093 (1980); see also A. Quattropani, F. Bassani, G. Margaritondo, and G. Tinivella, Nuovo Cimento **51B**, 335 (1979).
[10]M. Altarelli and D. L. Dexter, Phys. Rev. Lett. **29**, 1100 (1972).
[11]H. P. Hjalmarson, H. B. Büttner, and J. D. Dow, Phys. Rev. B **24**, 6010 (1981).
[12]C. Benndorf, H. Caus, B. Egert, H. Seidel, and F. Thieme, J. Electron Spectrosc. Relat. Phenom. **19**, 77 (1980).
[13]J. Stöhr, R. Jaeger, J. Feldhaus, S. Brennan, D. Norman, and G. Apai, Appl. Opt. **19**, 3911 (1980).
[14]C. Bonnelle, J. Phys. (Paris) Colloq. **28**, C3-65 (1967).
[15]We are greatly indebted to Professor A. Compaan of Kansas State University for supplying the single crystal.
[16]W. Gudat and C. Kunz, Phys. Rev. Lett. **29**, 169 (1972).
[17]J. Cerino, J. Stohr, N. Hower, and R. Z. Bachrach, Nucl. Instrum. Methods **172**, 227 (1980).
[18]J. Haber, T. Machej, L. Ungier, and J. Ziolkowski, J. Solid State Chem. **25**, 207 (1978); see also *Handbook x-ray Photoelectron Spectroscopy,* edited by G. E. Muilenberg (Perkin Elmer Corp., Eden Prairie, Minnesota, 1979).
[19]G. Schon, Surf. Sci. **35**, 96 (1973).
[20]G. Wertheim and S. Hufner, Phys. Rev. Lett. **28**, 1028 (1972).
[21]T. M. Zimkina and V. A. Fomichev, Dokl. Akad. Nauk SSSR **169**, 1304 (1966) [Sov. Phys. Dokl. **11**, 726 (1966)].
[22]J. L. Dehmer, J. Chem. Phys. **56**, 4496 (1972).
[23]C. R. Natoli, D. K. Misemer, S. Doniach, and F. W. Kutzler, Phys. Rev. A **22**, 1104 (1980); see also F. W. Kutzler, C. R. Natoli, D. K. Misemer, S. Doniach, and K. O. Hodgson, J. Chem. Phys. **73**, 3274 (1980), and A. Bianconi, S. Doniach, and D. Lublin, Chem. Phys. Lett. **59**, 121 (1978).
[24]P. J. Durham, J. B. Pendry, and C. H. Hodges, Comput. Phys. Commun. **25**, 193 (1982).
[25]J. B. Pendry, Comments Solid State Phys. **10**, 219 (1983).
[26]Y. Cauchois and N. F. Mott, Philos. Mag. **40**, 1260 (1949).
[27]N. N. Saxena, J. Phys. C **8**, 1450 (1975).
[28]B. G. Agarwal, C. B. Bhargava, A. N. Vishnoi and V. P. Seth, J. Phys. Chem. Solids **37**, 725 (1976).
[29]S. T. Pantelides and F. C. Brown, Phys. Rev. Lett. **33**, 298 (1974).
[30]A. Zunger, Phys. Rev. Lett. **50**, 1215 (1983).
[31]W. Scheifley, F. C. Brown, and S. T. Pantelides, in *Vacuum Ultraviolet Radiation Physics,* edited by E. Koch, R. Haensel, and C. Kunz (Pergamon-Vieweg, Braunschweig, 1974), p. 396.
[32]J. P. Stott, S. L. Hulbert, F. C. Brown, B. Bunker, T. C. Chiang, T. Miller, and K. H. Tan, Phys. Rev. B **30**, 2163 (1984).
[33]P. Keegstra and A. B. Kunz (private communication).